Organic Solar Cells

How to cite:
International Edition: doi.org/10.1002/anie.202013053
German Edition: doi.org/10.1002/ange.202013053

17.1%-Efficient Eco-Compatible Organic Solar Cells from a Dissymmetric 3D Network Acceptor

Hui Chen+, Hanjian Lai+, Ziyi Chen+, Yulin Zhu, Huan Wang, Liang Han, Yuanzhu Zhang, and Feng He*

Abstract: *To elevate the performance of polymer solar cells (PSC) processed by non-halogenated solvents, a dissymmetric fused-ring acceptor BTIC-2Cl-γCF_3 with chlorine and trifluoromethyl end groups has been designed and synthesized. X-ray crystallographic data suggests that BTIC-2Cl-γCF_3 has a 3D network packing structure as a result of H- and J-aggregations between adjacent molecules, which will strengthen its charge transport as an acceptor material. When PBDB-TF was used as a donor, the toluene-processed binary device realized a high power conversion efficiency (PCE) of 16.31%, which improved to 17.12% when PC71ThBM was added as the third component. Its efficiency of over 17% is currently the highest among polymer solar cells processed by non-halogenated solvents. Compared to its symmetric counterparts BTIC-4Cl and BTIC-CF_3-γ, the dissymmetric BTIC-2Cl-γCF_3 integrates their merits, and has optimized the molecular aggregations with excellent storage and photo-stability, and also extending the maximum absorption peak in film to 852 nm. The devices exhibit good transparency indicating a potential utilization in semi-transparent building integrated photovoltaics (ST-BIPV).*

Introduction

Continuous advances in new materials and device processes improve the power conversion efficiency (PCE) of polymer solar cells (PSC).[1–10] With the emergence of fused-ring acceptors, the PCEs of such devices increased to 18%,[11,12] approaching commercial levels in the organic photovoltaic field. From the viewpoint of practical commercial applications and industrial mass production, the technology of PSC processing should be carefully evaluated. Halogen-free solvents are an essential prerequisite for environmentally friendly and sustainable industrial applications. But regrettably, halogenated solvents, such as chloroform[13–16] and chlorobenzene,[11,17] are widely used currently in the fabrication of efficient PSCs. These solvents are good solvents for both donor and acceptor materials, and the resulting active film has nice morphology with a favourable nano-interpenetrated network, which is beneficial to the charge separation and transport.[13,14] These solvents are however highly toxic, and could be hazardous to the health of researchers. They evaporate into the atmosphere, causing pollution and harm to the environment. And the large-scale production and industrial application of halogenated solvents in preparation of PSCs is contrary to the current purpose of green chemistry. Recently, with the emergence of specifically designed donors and acceptors, some outstanding PSCs processed with eco-compatible solvents have been reported,[18–22] but the photovoltaic systems processed with halogen-free solvents were far less efficient than those processed with halogen-containing solvents. Processing of PSCs with minimally or non-toxic non-halogenated aromatic green solvents is necessary to support the commercial production of PSCs.[23,24]

In the development of PSCs processed by halogen-free solvents, new acceptor materials should be designed which balances the intermolecular interactions of the end groups and the centre fused cores. Accordingly, we explored molecules with the appropriate solubility in eco-compatible solvents. For most acceptors, end group modification is a flexible and effective way to broaden the absorption spectrum and fine-tune energy levels,[25–28] and it may also gradually change their processing capabilities in different solvents. Chlorine atoms have been successfully introduced into the end groups of non-fullerene acceptors, delivering many advances.[29–32] Chlorine shows the second largest electrophilic among the halogens and its empty 3d orbitals can accommodate lone pairs of electrons and/or π electrons to enter into extra non-covalent interactions, which could endow chlorine with intermolecular interactions stronger than those possessed by fluorine. Thus, chlorine, with a function similar to that of fluorine in organic optoelectronic materials, is even better in materials where the steric hindrance from its large atom size can be tolerated. The size of a chlorine atom could be overlooked when it is installed at the end of fused-ring

---

[*] Dr. H. Chen,[+] Dr. H. Lai,[+] Z. Chen,[+] Y. Zhu, H. Wang, L. Han, Prof. Y. Zhang, Prof. F. He
Shenzhen Grubbs Institute and Department of Chemistry, Southern University of Science and Technology
Shenzhen, 518055 (China)
E-mail: hef@sustech.edu.cn

Dr. H. Chen[+]
Academy for Advanced Interdisciplinary Studies, Southern University of Science and Technology
Shenzhen, 518055 (China)

Dr. H. Lai[+]
School of Chemistry and Chemical Engineering, Harbin Institute of Technology
Harbin, 150001 (China)

Prof. F. He
Guangdong Provincial Key Laboratory of Catalysis, Southern University of Science and Technology
Shenzhen, 518055 (China)

[+] These authors contributed equally to this work.

Supporting information and the ORCID identification number(s) for the author(s) of this article can be found under: https://doi.org/10.1002/anie.202013053.

electron acceptor systems. X-ray data shows that chlorinated fused-ring electron acceptors, such as ITIC-2Cl-γ, have a 3D network packing structure that depends on strong Cl···S and Cl···π interactions.[31] The improved order and crystallinity of species in such materials are very favourable for charge transport, and ITIC-2Cl-γ based PSCs have excellent PCE in a typical ITIC-system. Recently, the chlorine-containing acceptor BTIC-4Cl (BTP-4Cl)[17] was shown to enhance the red shift in its spectrum relative to BTP-4F (Y6).[10] The corresponding PSCs achieve efficiency of over 16 % with very high open-circuit voltages (V_{oc}) and a short-circuit current density (J_{sc}) attributable to their very low non-radiative energy loss. In most cases however, the solubility of those chlorinated acceptors will decrease as the number of chlorine atoms increases. As a result, to achieve decent PCEs, chloroform or chlorobenzene must be selected as the processing solvent.

Trifluoromethyl groups have also been successfully implanted in nonfullerene acceptors, and in our previous study, we reported an acceptor named BTIC-CF_3-γ.[26] The introduction of trifluoromethyl end groups did not disturb the molecular packing and crystalline. BTIC-CF_3-γ forms a 3D network structure as a result of the strong electrostatic attractions of the CF_3 end groups. With more isotropic features in the acceptor phase this facilitates the charge transport greatly and increases the efficiency of photovoltaic devices. At the same time, the solubility of BTIC-CF_3-γ is much better, such as in toluene and other non-halogenated solvents. To summarize, chlorination or trifluoromethylation can lead to 3D network structures with the capability of efficient charge transport in the acceptor phase. Multiple chlorine substitution is incompatible with eco-compatible solvent processing which delivers acceptors with high solar conversion efficiency due to the strong noncovalent interactions. In contrast, trifluoromethylation produces an opposite effect albeit with slightly less efficiency. In order to combine the advantages of both chlorination and trifluoromethylation and generate a highly efficient fused-ring acceptor in eco-compatible solvent conditions, the dissymmetric strategy led us to develop a new molecular design with one of these two functional groups at one end of the fused core and the second at the other end. The combined intermolecular interactions from these two end groups make a final molecule which is sufficiently soluble in most solvents, even halogen-free solvents, thus facilitating the eco-compatible processing requirements.

Therefore, a dissymmetric fused-ring acceptor, BTIC-2Cl-γCF_3 was designed and synthesized according to the theory of end group optimization. It showed good solubility in toluene, and its spin-coated film exhibited red-shifted absorption with a maximum peak at 852 nm and an on-set peak of ≈ 947 nm. The single crystal diffraction pattern of BTIC-2Cl-γCF_3 indicated that multiple intermolecular interactions such as F···S, F···O, F···N, Cl···S, Cl···O, N···O and N···S exist in the solid state of acceptor, and in addition, synergistic H- and J-aggregations were also found. As a result, a 3D network packing structure was formed, affording more electronic transition channels.[26,31] When using the polymer PBDB-TF as donor, PSCs processed with chlorobenzene, xylene or toluene, all delivered excellent photovoltaic performance. The toluene-processed binary device had a high PCE of 16.31 %, and the ternary device when processed in toluene with an implanted fullerene derivative PC_{71}ThBM as the third component gained a higher PCE up to 17.12 %, simultaneously improving the V_{oc}, J_{sc} and FF compared to the corresponding binary device. This is the first report of a PCE > 17 % prepared with processing with halogen-free solvents. The ternary device had favourable charge transport properties and elevated the response from 450 to 600 nm and 670 to 830 nm in external quantum efficiency (EQE) spectrum. From the investigated morphology and transient dynamics of the carrier it could be seen that the ternary device possesses a tailored crystallite size and ultra-low bimolecular recombination. Benefitting from the low bandgap absorption feature, BTIC-2Cl-γCF_3-based semi-transparent PSCs (ST-PSC) with 15 nm Ag also presented a very high PCE of 13.06 % with an average visible transmittance (AVT) of 24.45 %, which is one of the highest values with decent light transmission reported to date. In brief, this molecular design combined with chlorination and trifluoromethylation approaches an ideal state for molecular aggregation, making this kind of acceptor a good candidate for future building of integrated photovoltaic (ST-BIPV) materials based on eco-compatible solvent processing.

Results and Discussion

Material Synthesis

The precursor BT-2CHO was produced according to previous published reports. The synthetic routes to BTIC-2Cl-γCF_3 are shown in Figure S1a, and the molecular structure of BTIC-4Cl, BTIC-CF_3-γ, BTIC-2Cl-γCF_3, PBDB-TF and PC_{71}ThBM are shown in Figure S1b and Figure 1a. The BTIC-2Cl-γCF_3 was obtained from BT-2CHO in a one-step reaction with sequentially added IC-2Cl and IC-CF3-γ at 50 °C for 6 h, and then purified by HPLC and recrystallization. The structures of all the products were confirmed by ^{1}H NMR spectroscopy. Detailed synthesis procedures and characterization are in the Supplementary Information. In a thermogravimetric analysis (TGA) test (Figure S2), the purified BTIC-2Cl-γCF_3 displayed a decomposition temperature of 328 °C and 5 % weight loss. Its good thermal stability ensured that the BTIC-2Cl-γCF_3 in the neat and blend film would not degrade during thermal annealing in the device processing. The UV/Vis absorption spectra of BTIC-2Cl-γCF_3, including solution and film states are shown in Figure 2a. In solution in toluene, BTIC-2Cl-γCF_3 has absorption bands from 600–800 nm, its λ_{max} is 742 nm and its absorption coefficient is $1.81\times10^5\ M^{-1}cm^{-1}$. Interestingly, the film of BTIC-2Cl-γCF_3 exhibited a redshift at $\lambda_{max} = 852$ nm, with an absorption coefficient of $1.36\times10^5\ cm^{-1}$. The film absorption range compared to that of the solution extended to 947 nm and the detailed optical properties are listed in Table S1. The data indicated that BTIC-2Cl-γCF_3 molecules have very strong aggregation in the film, leading to the red shift and extension of the absorption spectrum. The absorption was

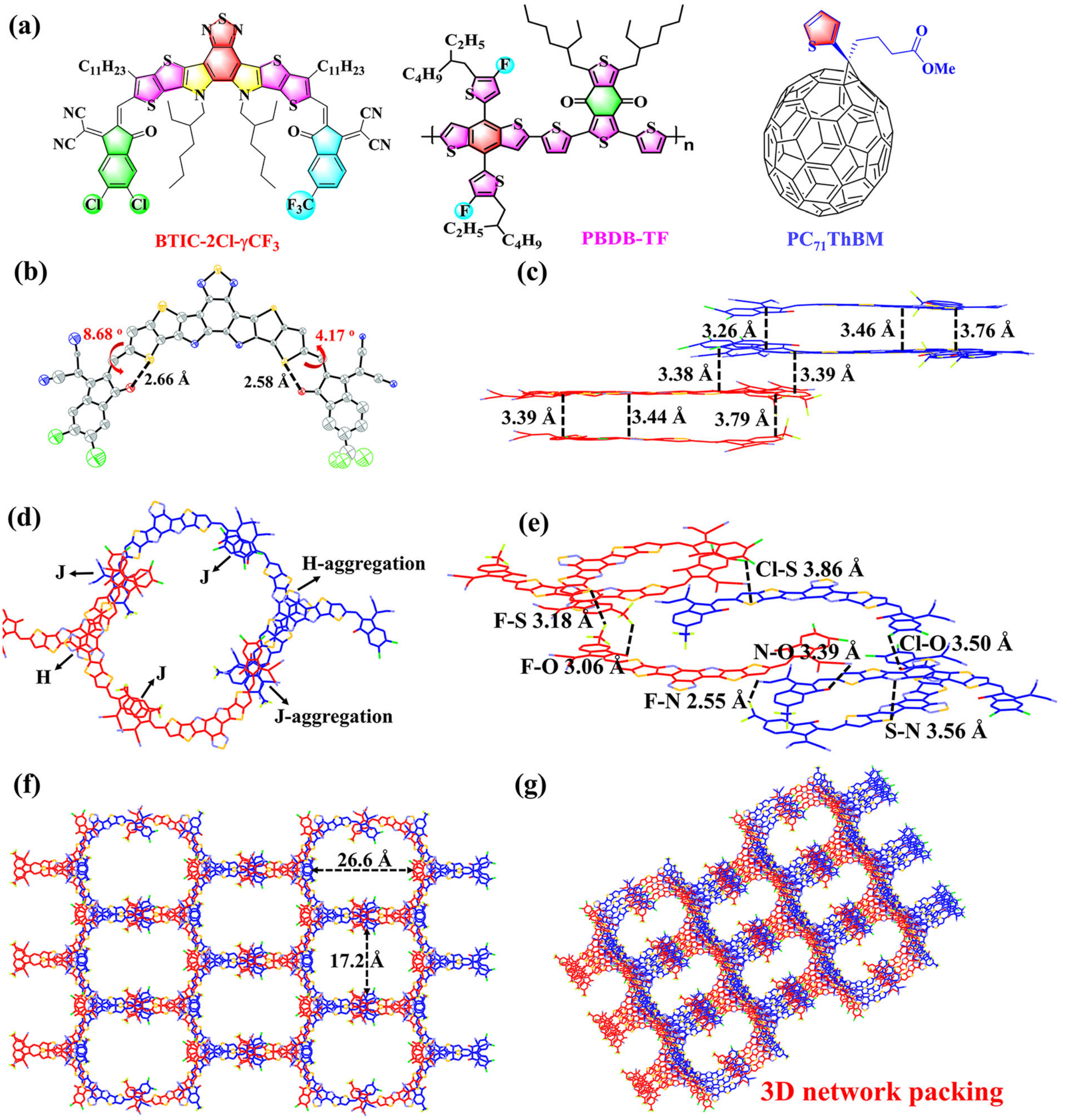

Figure 1. a) The molecular structures of BTIC-2Cl-γCF_3, PBDB-TF, and PC_{71}ThBM, respectively; b) the single-crystal structure of BTIC-2Cl-γCF_3, for the CCDC number see the Supporting Information, c) the π···π interactions in one elliptical frame, d) the single-crystal structure of one elliptical frame, e) the intermolecular interactions in one elliptical frame, f) 3D network packing from the c-crystallographic axis, g) the 3D network packing from c*-crystallographic axis. (The alkyl chains of BTIC-2Cl-γCF_3 were omitted to clearly observe the packing details).

very complementary to that of other polymer donors with wide-band energy gap, the BTIC-2Cl-γCF_3 based PSCs should have efficient light harvesting to deliver a high J_{sc} in devices. Thus, it appears that a designed BTIC-2Cl-γCF_3 acceptor is a potential candidate for high performance PSCs.

Packing information

The X-ray single crystal structure of BTIC-2Cl-γCF_3 was determined to reveal its packing information in the solid state.[26,31–35] Figure 1b shows the monomolecular state of BTIC-2Cl-γCF_3 from a top view. The torsional angles are 4.17° for the trifluoromethylated side and 8.68° for the chlorinated side, and there is a S···O=C conformational lock 2.58 Å and 2.66 Å in length. The packing information is shown in Figures 1c,d and e. Each elliptical frame structure consists of six molecules with multiple intermolecular interactions, including π···π interactions between end groups (J-aggregations), π···π interactions between cores (H-aggregations),[36] and non-covalent interactions including F···S, F···O, F···N, Cl···S, Cl···O, N···O and N···S. The specific values are displayed in Figure S3. As a result, a 3D network packing structure was achieved and comprised of multiple elliptical

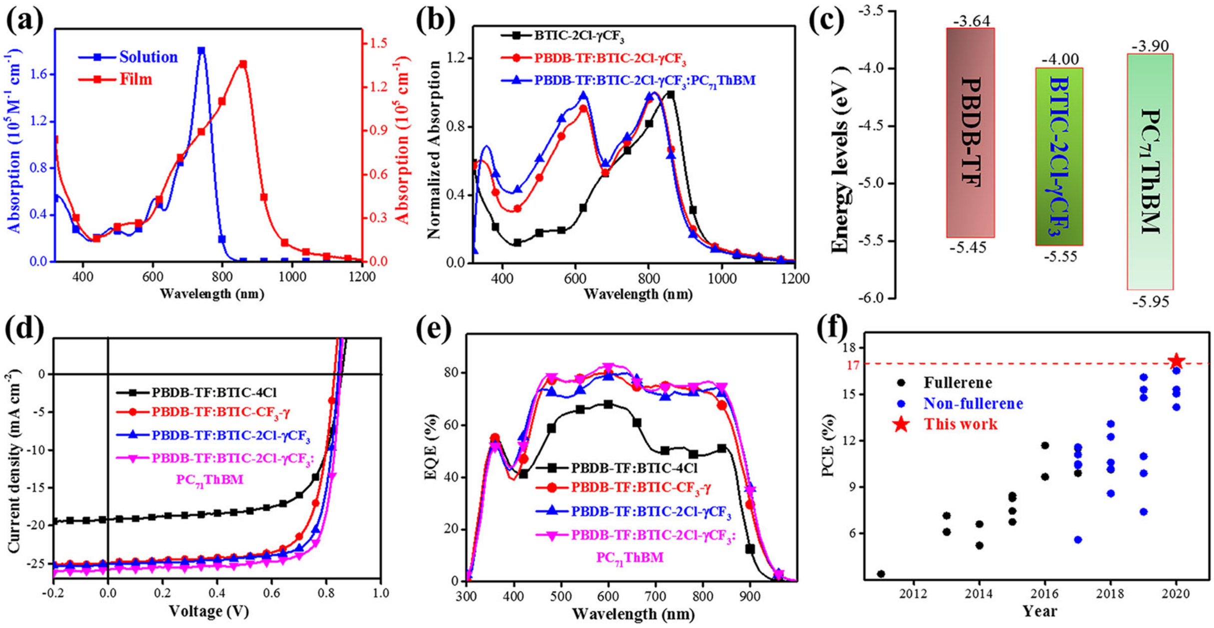

Figure 2. a) Absorption spectra of BTIC-2Cl-γCF$_3$ in solution and film. b) Normalized absorptions of BTIC-2Cl-γCF$_3$ neat film, related binary and ternary films. c) The molecular energy levels of PBDB-TF, BTIC-2Cl-γCF$_3$, and PC$_{71}$ThBM. d) *J*–*V* curves of BTIC-4Cl, BTIC-CF$_3$-γ, BTIC-2Cl-γCF$_3$, and BTIC-2Cl-γCF$_3$:PC$_{71}$ThBM based PSCs processed by toluene. e) EQE curves of corresponding devices. f) Recent advances in PSCs processed in halogen-free solvents.

frames with a length of 26.6 Å and a width of 17.2 Å due to these intermolecular interactions. More crystal details are shown in supplementary information (Figures S4–6). The 3D network packing of BTIC-2Cl-γCF$_3$ provides more electronic hoping channels for charge transfer in a variety of directions. We think that the acceptor with 3D network packing structure is beneficial to the performance of the molecule itself, so as to further improve the performance of final devices.

Photovoltaic Performance

To fabricate efficient BTIC-2Cl-γCF$_3$ PSCs, the desired polymer donor PBDB-TF was selected through matched optoelectronic properties.[17] The pure absorptions of the neat and blended films are shown in Figure 2b. Their energy levels further supported the device preparation from Figure 2c. Electrochemical cyclic voltammetry (CV) measurements were used to determine the energy levels of BTIC-2Cl-γCF$_3$ as shown in Figure S7. The well-screened absorption spectra and their energy levels were beneficial to production of high V_{oc} and J_{sc} in their PSCs. In order to systematically study the photovoltaic performance of BTIC-2Cl-γCF$_3$, conventional devices were fabricated and processed by different solvents such as chlorobenzene, xylene and toluene. The detailed device configuration and fabrication are described in the supporting information. Although the reported BTIC-4Cl and BTIC-CF$_3$-γ had excellent photovoltaic performance,[17,26] the toluene-processed BTIC-4Cl based PSCs showed a moderate PCE of 11.14%, with a higher V_{oc} of 0.86 V. The J_{sc} was quite low; while toluene-processed BTIC-CF$_3$-γ-based PSCs (Figure 2d) had a PCE of 15.10% (Table 1). These results implied that the toluene-processed BTIC system with trifluoromethylation could be suitable to obtain good photovoltaic performance. Through this dissymmetric strategy, the novel BTIC-2Cl-γCF$_3$ could have the merits of both BTIC-4Cl and BTIC-CF$_3$-γ. The BTIC-2Cl-γCF$_3$ based binary device with different processing solvents both had good PCEs. In particular, the toluene-processed binary device revealed an excellent PCE of 16.31%, with V_{oc} of 0.84 V, a high J_{sc} of 25.09 mA cm^{-2} and an FF of 76.99%, as shown in Table 1. The corresponding current density-voltage (*J*–*V*) curve of the device is presented in Figure 2d, and the *J*–*V* curves and performance parameters of devices processed by chlorobenzene and xylene are presented in Figure S8 and Table S2. To promote the higher PCE, a ternary blend strategy was conducted, which has been extensively studied and has made encouraging progress.[37–40] By introducing a third ingredient with customized absorption and energy levels to the binary film, the cascade energy levels and optimized morphology caused facilitate charge transfer in the ternary device and improve the performance of PSCs. In this binary system, several fullerene derivatives (Figure 1 and Figure S1b) were chosen as third components, and the resulting ternary PSCs had a better performance as shown in Figure S9 and Table S3. In ternary PSCs with PC$_{71}$ThBM, the device has simultaneously improved V_{oc}, J_{sc} and FF, resulting in a very high PCE of 17.12%. The detailed parameters are summarized in Table 1 and the *J*–*V* curve is shown in Figure 2d. Figure 2f lists recent advances PSCs processed in non-halogenated solvents (Table S4). This illustrates that the PCE of 17.12% is a record for PSCs processed by non-halogenated solvents. The PC$_{71}$ThBM had somewhat higher LUMO level compared to BTIC-2Cl-γCF$_3$, and that the PC$_{71}$ThBM as a fullerene derivative has high electron mobility. The same ternary method was also appropriate for

Table 1: The performance parameters of BTIC-4Cl, BTIC-CF$_3$-γ, BTIC-2Cl-γCF$_3$ and BTIC-2Cl-γCF$_3$:PC$_{71}$ThBM based PSCs processed with toluene under 100 mW cm^{-2} AM 1.5 G irradiation.

Acceptors	V_{oc} [V]	J_{sc} [mA cm^{-2}]	J_{Cal} [mA cm^{-2}]	FF [%]	PCE [%]
BTIC-4Cl	0.86 (0.86 ± 0.002)[a]	18.73 (18.52 ± 0.19)	18.42	69.27 (75.36 ± 0.60)	11.14 (10.83 ± 0.26)
BTIC-CF$_3$-γ	0.83 (0.83 ± 0.001)	24.88 (24.59 ± 0.28)	24.10	73.21 (72.52 ± 0.65)	15.10 (14.85 ± 0.18)
BTIC-2Cl-γCF$_3$	0.84 (0.84 ± 0.001)	25.09 (24.79 ± 0.24)	24.18	76.99 (76.16 ± 0.80)	16.31 (16.01 ± 0.27)
BTIC-2Cl-γCF$_3$: PC$_{71}$ThBM	0.85 (0.85 ± 0.001)	25.76 (25.43 ± 0.31)	24.96	78.10 (77.30 ± 0.75)	17.12 (16.75 ± 0.36)

[a] Average value ± standard deviation, calculated from 10 independent devices.

chlorobenzene and xylene-processed devices, the relevant *J–V* curves and performance parameters are also shown in Figure S8 and Table S2. BTIC-2Cl-γCF$_3$-based PSCs processed with non-halogenated solvents such as and toluene and xylene exhibit a high PCE, showing that BTIC-2Cl-γCF$_3$ is very promising commercial photovoltaic material from the aspect of the environment.

To understand and explore the origin of the high J_{sc} in binary and ternary devices, their EQE and absorption of blend film were determined and are shown in Figures 2 e and b, respectively. The binary blend films feature two absorption peaks from contributions of the PBDB-TF donor and the BTIC-2Cl-γCF$_3$ acceptor. The BTIC-2Cl-γCF$_3$ in the blend caused a peak at 818 nm and an obvious blue-shift compared with the peak from the BTIC-2Cl-γCF$_3$ neat film at 852 nm. This implies that the blends form a bulk-heterojunction breaking the molecular aggregation of BTIC-2Cl-γCF$_3$, and accelerating the separation of excitons in the interface between donor and acceptor. The ternary blend film with a minor amount of PC$_{71}$ThBM maintained the profile of a binary film, but the absorption range of 400 to 600 nm was somewhat increased. These are the reasons for the high J_{sc} generation in the devices. Although the EQE values of binary devices presented a good response from 450 to 830 nm, this interval fluctuated. As expected, the ternary device elevated the response from 450 to 600 nm and 670 to 830 nm in the EQE spectrum. The calculated J_{Cal} (Table 1) from EQE curves matched well with values of J_{sc} from *J–V* measurements. In consideration of ternary device with higher J_{sc} and FF, it should have favourable charge transport. As presented in Figure S10 and Table S5, the hole and electron mobility of devices were determined by a space-charge-limited current (SCLC) method.[41] The calculated hole/electron mobility were $2.1/1.5\times10^{-4}$ and $3.4/2.8\times10^{-4}$ cm^2 V^{-1} s^{-1} for the binary and ternary films, respectively. The charge accumulation could be reduced via the high and balance of charge transport in device. Thus, the ternary devices had higher J_{sc} and FF than those in binary devices.

Investigation of Charge Dynamics and Energy Loss

To understand the exciton quenching in binary and ternary devices, the photoluminescence (PL) spectra of neat, binary and ternary blend films were recorded and are shown in Figure 3 a. The neat film of BTIC-2Cl-γCF$_3$ has a typical PL emission peak around 940 nm. When blended with PBDB-TF donor, the curve of binary blend film had apparently no properties indicating high PL quenching efficiency. When the PC$_{71}$ThBM was introduced, the ternary blend film displayed a similar profile, and the intensity of PL was lower than that of the binary blend film. The results demonstrated that binary and ternary blend films both had a more efficient charge transfer behaviour,[42] and which of the ternary blend films was superior. The test of PL was accorded with the high EQE response of the ternary device, further supporting the higher J_{sc} and FF of the ternary device. To understand the bimolecular recombination of the carrier in the device, an examination of J_{sc} versus light intensity was conducted and the results are shown in Figure 3 b. J_{sc} and I could follow a relationship of $J_{sc}\propto I^{\alpha}$, where the slope α was calculated from the double-logarithmic coordinates curve.[43] The extracted values of binary and ternary devices were 0.98 and 0.99, respectively. These favourable consequences illustrated that they were both restrained in their bimolecular recombination. The ternary device possessed ultra-low bimolecular recombination and this corresponds with the high FF.

The energy loss, especially in non-radiative energy loss, is a key factor to limit the PCE of PSCs.[44] To detailed investigate the V_{oc} loss of binary and ternary devices, the optical gap of device (E_g^{PV}), highly sensitive EQE and electroluminescence (EL) quantum efficiencies (EQE$_{\mathrm{EL}}$) were measured in Figure S11, Figures 3 c and d, respectively. The systematic parameters of energy loss in devices were summarized in Table S6. The determined of binary and ternary devices were 1.448 and 1.450 eV, respectively.[45] The close E_g^{PV} resulted the very adjacent ΔE_1 of binary (0.267 eV) and ternary (0.268 eV) devices according to the Shockley-Queisser (SQ) limitation.[17,45] The efficient binary and ternary devices had similar highly sensitive EQE curves, but the evaluated ΔE_2 of ternary device was slightly lower than that of binary device. The ΔE_3 is non-radiative energy loss, which could be deduced from the equation $\Delta E_3 = -kTIn(\mathrm{EQE}_{\mathrm{EL}})$.[44] The binary and ternary devices both exhibited a high EQE$_{\mathrm{EL}}$ values, which were 8.9×10^{-5} and 1.1×10^{-4}, respectively. The high EQE$_{\mathrm{EL}}$ value is corresponding the low, indicating small non-radiative energy loss in related device. The extracted of binary device is 0.244 eV. When applied the ternary blend strategy, the of binary device was declined to 0.240 eV, further suppress non-radiative

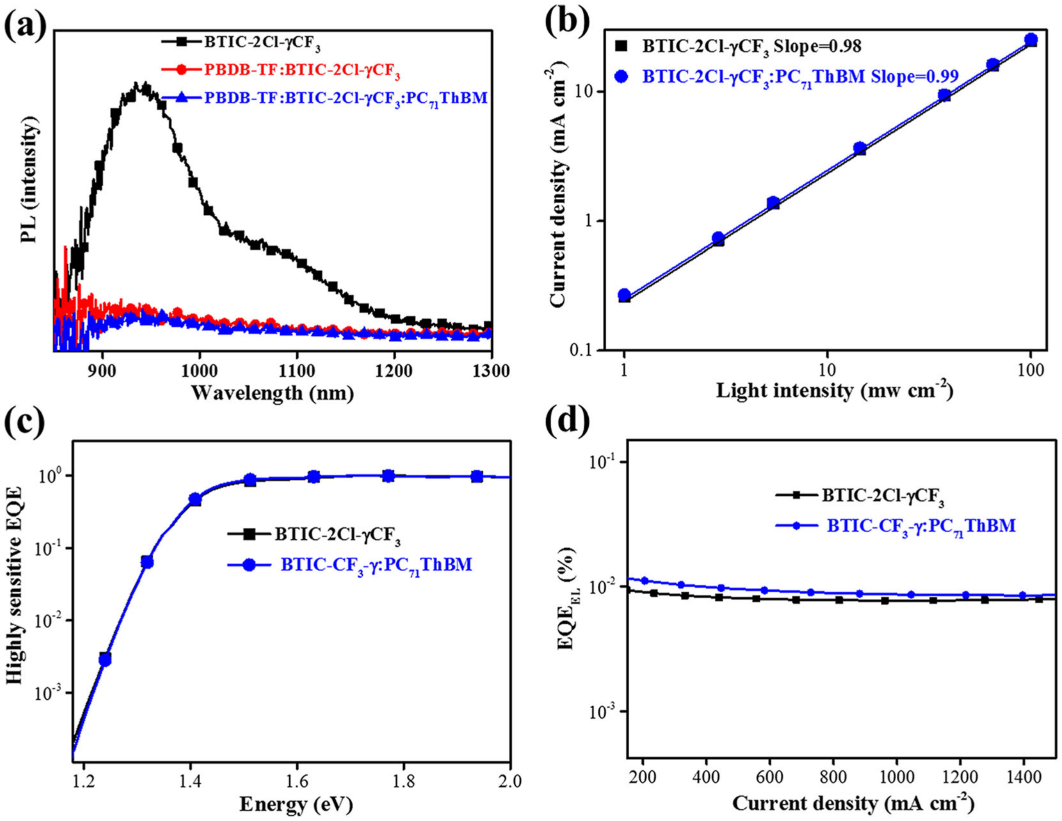

Figure 3. a) The PL spectra of neat, binary and ternary blend films, b) experimental J_{sc} versus light intensity. c) High sensitive EQE and d) EL quantum efficiencies for binary and ternary PSCs processed by toluene.

energy loss in devices.[17] The integrated ΔE of ternary device was 0.559 eV, which was lower than that of binary device (0.604 eV). Thus, the ternary device had an improved V_{oc} due to the cascading energy level and minimized energy loss, resulting a high PCE compared to the binary device. The dissymmetric 3D network acceptor broadened the absorption to achieve high J_{sc}, meanwhile, the non-radiative energy losses of BTIC-2Cl-γCF_3 based devices with high V_{oc} were also low, contributing the outstanding PCE of PSCs processed by toluene.

Morphology and Stability

The exciton dissociation and charge transport are closely related to the film morphology of active layer, including the phase separation scale, molecular packing and orientation, crystallinity and miscibility, all of which greatly affect the device performance.[46,47] Grazing incident wide-angle X-ray scattering (GIWAXS) was used to investigate the orientation of the molecular packing in the films. The binary and ternary films had the similar diffraction patterns, shown in Figures 4a and b.

From the out-of-plane line-cuts in Figure 4c, the characteristic π-π stacking peaks of binary and ternary films were found to be at 1.62 and 1.64 Å^{-1}, respectively, and the minor differences could be ignored. Their calculated full width at half-maximum (FWHM) were also very close. Thus, in the binary and ternary films, the molecular packing that dominates is in the face-on orientation, and the related device had favourable charge transport. In Figure 4d, the lamellar (100) diffraction peaks are around 0.30 Å^{-1} in the in-plane (IP) direction, but the FWHM of binary and ternary films were 0.03 Å^{-1} and 0.05 Å^{-1}, respectively. The smaller FWHM implied that there was a larger crystalline form in the binary film. This phenomenon indicates that the addition of PC_{71}ThBM further interrupted the aggregation of BTIC-2Cl-γCF_3 and suppressed its crystallinity.[43] An appropriately tailored crystallite size facilitates charge transport, consistent with the high J_{sc} and FF of the device. We also analysis the GIWAXS data combining with single crystal data. Figure S4 shows the powder *x*-ray diffraction pattern generated from single crystal data from BTIC-2Cl-γCF_3, it was found strong signals of $2\theta = 6.08°$, 7.16° and 26.48°, the corresponding distances are 14.52, 12.34, and 3.36 Å according to the Bragg equation $2d\sin\theta = \lambda$ in XRD, respectively, and the q value are 0.29, 0.51, and 1.87 Å^{-1} according to $d = 2\pi/q$, respectively. From the GIWAXS data, we found a set of values $q = 0.29$ and 0.53 Å^{-1} in the IP direction and $q = 1.87$ Å^{-1} in the OOP direction by the binary film, which is matching well with the data from single crystal, indicating that the packing modes of BTIC-2Cl-γCF_3 should be partially reserved in the blend film.[29,34]

We used atomic force microscopy (AFM) to further explore the surface morphology of the film in Figure S12. The binary and ternary films had a root mean square (RMS) of 1.28 and 1.39 nm, respectively. Both had smooth and uniform surface morphology, forming beneficial contact with the

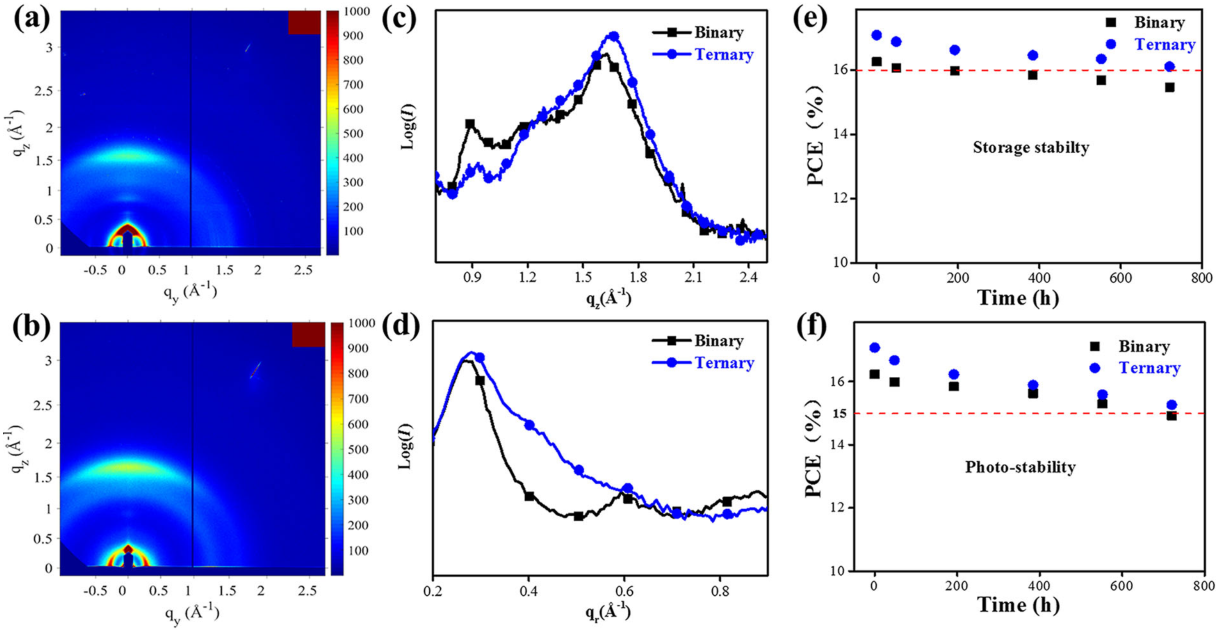

Figure 4. GIWAXS patterns of binary (a) and ternary films (b), the corresponding line-cuts in the out-of-plane (c) and in-plane (d). The storage stability (e) and photo-stability (f) of devices from toluene processing.

interface and facilitating the performance of the device.[42] The transmission electron microscopy (TEM) images of binary and ternary films exhibited the appropriate phase separation and nanoscale fibre in Figure S13. The favourable morphology caused the device to have excellent stability. The storage and photo-stability were both tested, and their decayed trends are presented in Figures 4e and 4f. The binary and ternary devices maintain 95% of the initial efficiency in a glovebox under nitrogen for 720 h, the absorption of binary and ternary films stored in a glovebox are without obvious decline from the Figures S14a and b. When the devices were continuously illuminated for some time in a nitrogen-filled glovebox, the PCE of ternary device was still over 15%. According to the time-dependent absorption of binary and ternary films under illumination in Figures S14c and d, the absorption of ternary films displayed a slower descend than that of binary films. Thus, the ternary film had more stability than binary film under illumination.[29] This excellent stability indicated that BTIC-2Cl-γCF_3 based photovoltaic systems should have a good commercial future.

Semi-transparent Devices

The low band-gap acceptor BTIC-2Cl-γCF_3 has strong absorption in the near-infrared region, and allows visible light to penetrate as much as possible. Light at non-visible wavelengths is absorbed and utilized by the active layer, thus improving the light transmission performance, and this will promote the PCE of ST devices.[47–50] The fabricated ST-PSCs had same structure and are processed as opaque devices, but the Ag electrode thickness was reduced to 10–20 nm. The thickness of Ag was calibrated by AFM in Figure S15. The *J–V*, EQE, transmittance and reflectance curves of toluene processed ST ternary devices are presented in Figures 5a–c and Figure S16, and the related performance parameters are summarized in Table 2. As the thickness of the Ag layer increased, J_{sc} and FF were obviously enhanced while the AVT decreased. For ST-PSC, there is a distinct trade-off between the AVT and PCE. Generally, when balancing the PCE and the transparency window application, the value of AVT is around 25%.[49] In this case, the ST device with 15 nm Ag showed a high PCE of 13.06%, with V_{oc} of 0.82 V, J_{sc} of 21.55 mA cm^{-2} and FF of 73.64%, under the AVT of 24.5% condition. Figure 5d and Table S7 list the PCEs over 10% based on ST-PSCs. In recent years, this work produced the highest performance ST-PSCs based on BTIC-2Cl-γCF_3 with an AVT around 25%. To quantify the visual appearance of fabricated ST-PSCs, the calculated colour coordinates (*x*, *y*) are shown in Figure 5e, and the coordinates of 10, 15 and 20 nm Ag ST devices were (0.29, 0.30), (0.26, 0.27) and (0.26, 0.6), respectively. Figure 5 f shows an outdoor image through the ST-PSCs. From the photograph, the ST devices exhibited good resolution, colour sense, and transparency, giving it only a slightly blue cast. These parameters indicated that BTIC-2Cl-γCF_3 is a very promising translucent photovoltaic material for ST-BIPV productions.

Conclusion

Utilizing the combined advantages of chlorination and trifluoromethylation, we have designed and synthesized a dissymmetric fused-ring acceptor, BTIC-2Cl-γCF3 with optimized molecular aggregation. Single crystal analysis indicated a 3D network packing structure in this dissymmetric acceptor which has improved charge transfer. The developed PSCs using PBDB-TF as donor, processed by chlorobenzene, xylene and toluene solvents, all achieved excellent photovoltaic performance. The toluene-processed binary device

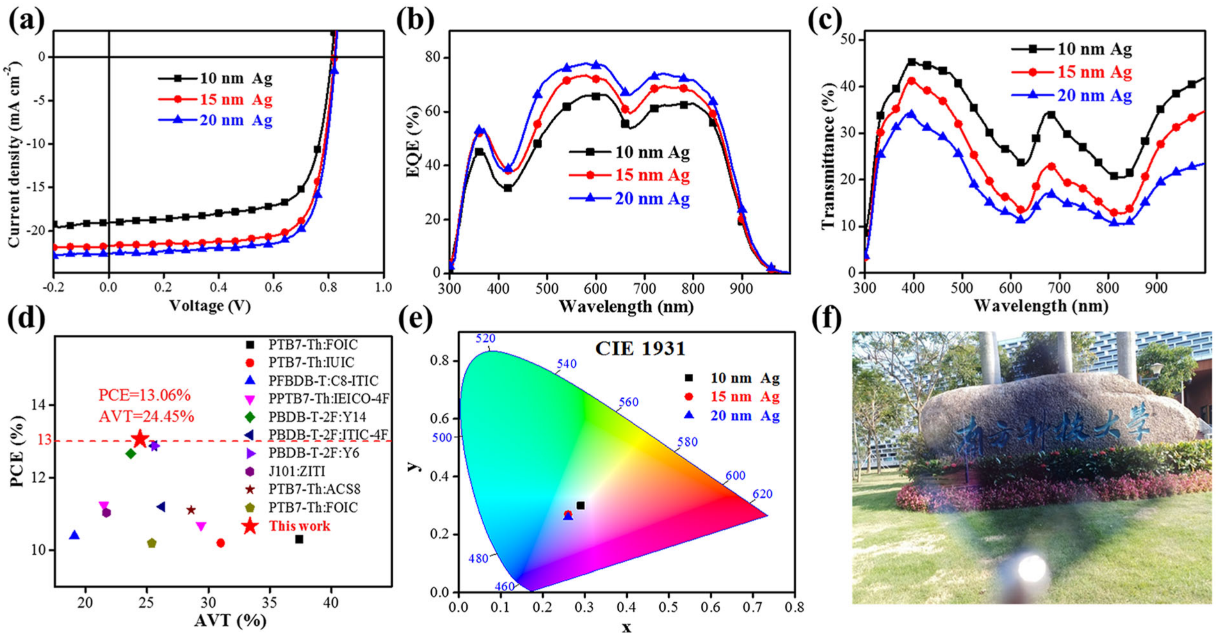

Figure 5. a) *J*–*V*, b) EQE, and c) transmission curves of toluene processed semi-transparent ternary devices with varied thickness of Ag cathode. d) The PCEs over 10% based on ST-PSCs in recent years. e) CIE coordinates of related devices, f) Outdoor image through the ST-PSCs.

Table 2: The performance parameters of toluene processed semi-transparent ternary PSCs with various Ag cathode thicknesses under 100 mW cm^{-2} AM 1.5 G irradiation.

Ag	V_{oc} [V]	J_{sc} [mA cm^{-2}]	J_{Cal} [mA cm^{-2}]	FF [%]	PCE [%]	AVT [%]
10 nm	0.81 (0.81 ± 0.001)[a]	19.04 (18.99 ± 0.10)	18.72	70.04 (68.34 ± 1.74)	10.82 (10.52 ± 0.28)	33.61
15 nm	0.82 (0.82 ± 0.001)	21.55 (21.24 ± 0.28)	20.78	73.64 (71.54 ± 1.87)	13.06 (12.81 ± 0.22)	24.45
20 nm	0.82 (0.82 ± 0.002)	23.03 (22.87 ± 0.17)	22.54	74.45 (72.82 ± 1.61)	14.13 (13.58 ± 0.43)	19.20

[a] Average value ± standard deviation were calculated from 10 independent devices.

had a high PCE of 16.31%, with PC71ThBM as a small amount of third component incorporated into original binary system, the produced ternary device with small non-radiative energy loss obtained a further higher PCE of 17.12%, which is the highest among PSCs processed with halogen-free solvent. The BTIC-2Cl-γCF3 based ST-PSCs have a PCE of 13.06% with an AVT of 24.45%, and are the best-performing devices with an AVT of around 25%, and show great potential for use in ST-BIPV productions. Our findings indicate that the dissymmetric strategy of chlorination and trifluoromethylation is a feasible method with which to develop promising photovoltaic materials, using eco-compatible efficient PSCs processed by halogen-free solvents.

Acknowledgements

This work was financially supported by the National Natural Science Foundation of China (21733005, 51903116, and 21975115), Shenzhen Fundamental Research program (JCYJ20170817111214740 and KQJSCX20180319114442157) and Shenzhen Nobel Prize Scientists Laboratory Project (C17783101), Guangdong Provincial Key Laboratory of Catalysis (2020B121201002), Guangdong Innovative and Entrepreneurial Research Team Program (2016ZT06G587) and Shenzhen Sci-Tech Fund (KYTDPT20181011104007). We thank Dr. Joseph Strzalka and Dr. Zhang Jiang for the assistance with GIWAXS measurements. Use of the Advanced Photon Source (APS) at the Argonne National Laboratory was supported by the U.S. Department of Energy, Office of Science, Office of Basic Energy Sciences, under contract No. DE-AC02-06CH11357. We also thank the SUSTech Core Research Facilities for the AFM and TEM measurements.

Conflict of interest

The authors declare no conflict of interest.

Keywords: 3D networks · chlorination · eco-compatible · non-fullerene acceptors · organic solar cells

[1] Z. He, B. Xiao, F. Liu, H. Wu, Y. Yang, S. Xiao, C. Wang, T. P. Russell, Y. Cao, *Nat. Photonics* **2015**, *9*, 174 – 179.

[2] C. Yan, S. Barlow, Z. Wang, H. Yan, A. K. Y. Jen, S. R. Marder, X. Zhan, *Nat. Rev. Mater.* **2018**, *3*, 18003.

[3] G. Li, R. Zhu, Y. Yang, *Nat. Photonics* **2012**, *6*, 153 – 161.

[4] Y. Li, *Acc. Chem. Res.* **2012**, *45*, 723 – 733.

[5] Y. Liu, J. Zhao, Z. Li, C. Mu, W. Ma, H. Hu, K. Jiang, H. Lin, H. Ade, H. Yan, *Nat. Commun.* **2014**, *5*, 5293.

[6] P. Cheng, G. Li, X. Zhan, Y. Yang, *Nat. Photonics* **2018**, *12*, 131 – 142.

[7] B. Fan, X. Du, F. Liu, W. Zhong, L. Ying, R. Xie, X. Tang, K. An, J. Xin, N. Li, W. Ma, C. J. Brabec, F. Huang, Y. Cao, *Nat. Energy* **2018**, *3*, 1051 – 1058.

[8] L. Meng, Y. Zhang, X. Wan, C. Li, X. Zhang, Y. Wang, X. Ke, Z. Xiao, L. Ding, R. Xia, H.-L. Yip, Y. Cao, Y. Chen, *Science* **2018**, *361*, 1094.

[9] P. Chao, H. Chen, Y. Zhu, H. Lai, D. Mo, N. Zheng, X. Chang, H. Meng, F. He, *Adv. Mater.* **2020**, *32*, 1907059.

[10] J. Yuan, Y. Zhang, L. Zhou, G. Zhang, H.-L. Yip, T.-K. Lau, X. Lu, C. Zhu, H. Peng, P. A. Johnson, M. Leclerc, Y. Cao, J. Ulanski, Y. Li, Y. Zou, *Joule* **2019**, *3*, 1140 – 1151.

[11] Y. Cui, H. Yao, J. Zhang, K. Xian, T. Zhang, L. Hong, Y. Wang, Y. Xu, K. Ma, C. An, C. He, Z. Wei, F. Gao, J. Hou, *Adv. Mater.* **2020**, *32*, 1908205.

[12] Q. Liu, Y. Jiang, K. Jin, J. Qin, J. Xu, W. Li, J. Xiong, J. Liu, Z. Xiao, K. Sun, S. Yang, X. Zhang, L. Ding, *Sci. Bull.* **2020**, *65*, 272 – 275.

[13] J. Lee, S.-J. Ko, H. Lee, J. Huang, Z. Zhu, M. Seifrid, J. Vollbrecht, V. V. Brus, A. Karki, H. Wang, K. Cho, T.-Q. Nguyen, G. C. Bazan, *ACS Energy Lett.* **2019**, *4*, 1401 – 1409.

[14] K. Jiang, Q. Wei, J. Y. L. Lai, Z. Peng, H. K. Kim, J. Yuan, L. Ye, H. Ade, Y. Zou, H. Yan, *Joule* **2019**, *3*, 3020 – 3033.

[15] B. Fan, D. Zhang, M. Li, W. Zhong, Z. Zeng, L. Ying, F. Huang, Y. Cao, *Sci. Chin. Chem.* **2019**, *62*, 746 – 752.

[16] Q. Wu, J. Guo, R. Sun, J. Guo, S. Jia, Y. Li, J. Wang, J. Min, *Nano Energy* **2019**, *61*, 559 – 566.

[17] Y. Cui, H. Yao, J. Zhang, T. Zhang, Y. Wang, L. Hong, K. Xian, B. Xu, S. Zhang, J. Peng, Z. Wei, F. Gao, J. Hou, *Nat. Commun.* **2019**, *10*, 2515.

[18] L. Ye, Y. Xiong, Q. Zhang, S. Li, C. Wang, Z. Jiang, J. Hou, W. You, H. Ade, *Adv. Mater.* **2018**, *30*, 1705485.

[19] Q. Fan, Q. Zhu, Z. Xu, W. Su, J. Chen, J. Wu, X. Guo, W. Ma, M. Zhang, Y. Li, *Nano Energy* **2018**, *48*, 413 – 420.

[20] R. Sun, T. Wang, Z. Luo, Z. Hu, F. Huang, C. Yang, J. Min, *Sol. RRL* **2020**, *4*, 2000156.

[21] L. Hong, H. Yao, Z. Wu, Y. Cui, T. Zhang, Y. Xu, R. Yu, Q. Liao, B. Gao, K. Xian, H. Y. Woo, Z. Ge, J. Hou, *Adv. Mater.* **2019**, *31*, 1903441.

[22] R. Yu, H. Yao, Y. Cui, L. Hong, C. He, J. Hou, *Adv. Mater.* **2019**, *31*, 1902302.

[23] C.-C. Chueh, K. Yao, H.-L. Yip, C.-Y. Chang, Y.-X. Xu, K.-S. Chen, C.-Z. Li, P. Liu, F. Huang, Y. Chen, W.-C. Chen, A. K. Y. Jen, *Energy Environ. Sci.* **2013**, *6*, 3241 – 3248.

[24] C. Sprau, F. Buss, M. Wagner, D. Landerer, M. Koppitz, A. Schulz, D. Bahro, W. Schabel, P. Scharfer, A. Colsmann, *Energy Environ. Sci.* **2015**, *8*, 2744 – 2752.

[25] Z. Luo, T. Liu, Y. Wang, G. Zhang, R. Sun, Z. Chen, C. Zhong, J. Wu, Y. Chen, M. Zhang, Y. Zou, W. Ma, H. Yan, J. Min, Y. Li, C. Yang, *Adv. Energy Mater.* **2019**, *9*, 1900041.

[26] H. Lai, Q. Zhao, Z. Chen, H. Chen, P. Chao, Y. Zhu, Y. Lang, N. Zhen, D. Mo, Y. Zhang, F. He, *Joule* **2020**, *4*, 688 – 700.

[27] Q. Zhang, M. A. Kelly, N. Bauer, W. You, *Acc. Chem. Res.* **2017**, *50*, 2401 – 2409.

[28] J. Qu, H. Chen, J. Zhou, H. Lai, T. Liu, P. Chao, D. Li, Z. Xie, F. He, Y. Ma, *ACS Appl. Mater. Interfaces* **2018**, *10*, 39992 – 40000.

[29] H. Chen, Z. Hu, H. Wang, L. Liu, P. Chao, J. Qu, W. Chen, A. Liu, F. He, *Joule* **2018**, *2*, 1623 – 1634.

[30] H. Zhang, H. Yao, J. Hou, J. Zhu, J. Zhang, W. Li, R. Yu, B. Gao, S. Zhang, J. Hou, *Adv. Mater.* **2018**, *30*, 1800613.

[31] H. Lai, H. Chen, J. Zhou, J. Qu, P. Chao, T. Liu, X. Chang, N. Zheng, Z. Xie, F. He, *iScience* **2019**, *17*, 302 – 314.

[32] H. Lai, H. Chen, J. Zhou, J. Qu, M. Wang, W. Xie, Z. Xie, F. He, *J. Phys. Chem. Lett.* **2019**, *10*, 4737 – 4743.

[33] T. J. Aldrich, M. Matta, W. Zhu, S. M. Swick, C. L. Stern, G. C. Schatz, A. Facchetti, F. S. Melkonyan, T. J. Marks, *J. Am. Chem. Soc.* **2019**, *141*, 3274 – 3287.

[34] G. Zhang, X. Chen, J. Xiao, P. C. Y. Chow, M. Ren, G. Kupgan, X. Jiao, C. C. S. Chan, X. Du, R. Xia, Z. Chen, J. Yuan, Y. Zhang, S. Zhang, Y. Liu, Y. Zou, H. Yan, K. Wong, V. Coropceanu, N. Li, C. J. Brabec, J. L. Bredas, H. L. Yip, Y. Cao, *Nat. Commun.* **2020**, *11*, 3943.

[35] S. Dai, J. Zhou, S. Chandrabose, Y. Shi, G. Han, K. Chen, J. Xin, K. Liu, Z. Chen, Z. Xie, W. Ma, Y. Yi, L. Jiang, J. M. Hodgkiss, X. Zhan, *Adv. Mater.* **2020**, *32*, 2000645.

[36] F. Würthner, T. E. Kaiser, C. R. Saha-Möller, *Angew. Chem. Int. Ed.* **2011**, *50*, 3376 – 3410; *Angew. Chem.* **2011**, *123*, 3436 – 3473.

[37] Y. Zhu, A. Gadisa, Z. Peng, M. Ghasemi, L. Ye, Z. Xu, S. Zhao, H. Ade, *Adv. Energy Mater.* **2019**, *9*, 1900376.

[38] H. Lu, J. Zhang, J. Chen, Q. Liu, X. Gong, S. Feng, X. Xu, W. Ma, Z. Bo, *Adv. Mater.* **2016**, *28*, 9559 – 9566.

[39] G. Zhang, K. Zhang, Q. Yin, X.-F. Jiang, Z. Wang, J. Xin, W. Ma, H. Yan, F. Huang, Y. Cao, *J. Am. Chem. Soc.* **2017**, *139*, 2387 – 2395.

[40] D. Baran, R. S. Ashraf, D. A. Hanifi, M. Abdelsamie, N. Gasparini, J. A. Röhr, S. Holliday, A. Wadsworth, S. Lockett, M. Neophytou, C. J. M. Emmott, J. Nelson, C. J. Brabec, A. Amassian, A. Salleo, T. Kirchartz, J. R. Durrant, I. McCulloch, *Nat. Mater.* **2017**, *16*, 363 – 369.

[41] P. N. Murgatroyd, *J. Phys. D* **1970**, *3*, 151 – 156.

[42] K. Kawashima, T. Fukuhara, Y. Suda, Y. Suzuki, T. Koganezawa, H. Yoshida, H. Ohkita, I. Osaka, K. Takimiya, *J. Am. Chem. Soc.* **2016**, *138*, 10265 – 10275.

[43] A. K. K. Kyaw, D. H. Wang, C. Luo, Y. Cao, T.-Q. Nguyen, G. C. Bazan, A. J. Heeger, *Adv. Energy Mater.* **2014**, *4*, 1301469.

[44] D. Qian, Z. Zheng, H. Yao, W. Tress, T. R. Hopper, S. Chen, S. Li, J. Liu, S. Chen, J. Zhang, X. Liu, B. Gao, L. Ouyang, Y. Jin, G. Pozina, I. A. Buyanova, W. M. Chen, O. Inganäs, V. Coropceanu, J. Bredas, H. Yan, J. Hui, F. Zhang, A. A. Bakulin, F. Gao, *Nat. Mater.* **2018**, *17*, 703 – 709.

[45] Y. Wang, D. Qian, Y. Cui, H. Zhang, J. Hou, K. Vandwal, T. Kirchartz, F. Gao, *Adv. Energy Mater.* **2018**, *8*, 1801352.

[46] W. Ma, J. R. Tumbleston, M. Wang, E. Gann, F. Huang, H. Ade, *Adv. Energy Mater.* **2013**, *3*, 864 – 872.

[47] Z. Hu, H. Chen, J. Qu, X. Zhong, P. Chao, M. Xie, W. Lu, A. Liu, L. Tian, Y.-A. Su, W. Chen, F. He, *ACS Energy Lett.* **2017**, *2*, 753 – 758.

[48] Y. Li, J.-D. Lin, X. Che, Y. Qu, F. Liu, L.-S. Liao, S. R. Forrest, *J. Am. Chem. Soc.* **2017**, *139*, 17114 – 17119.

[49] Y. Bai, C. Zhao, X. Chen, S. Zhang, S. Zhang, T. Hayat, A. Alsaedi, Z. A. Tan, J. Hou, Y. Li, *J. Mater. Chem. A* **2019**, *7*, 15887 – 15894.

[50] W. Song, B. Fanady, R. Peng, L. Hong, L. Wu, W. Zhang, T. Yan, T. Wu, S. Chen, Z. Ge, *Adv. Energy Mater.* **2020**, *10*, 2000136.

Manuscript received: September 27, 2020
Accepted manuscript online: October 23, 2020
Version of record online: ■■ ■■, ■■■■

Research Articles

Organic Solar Cells

H. Chen, H. Lai, Z. Chen, Y. Zhu,
H. Wang, L. Han, Y. Zhang,
F. He* ——————— ■■■■–■■■■

17.1%-Efficient Eco-Compatible Organic Solar Cells from a Dissymmetric 3D Network Acceptor

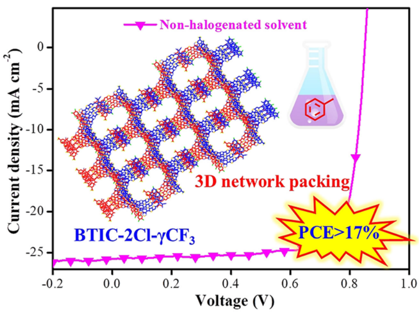

A dissymmetric fused-ring acceptor BTIC-2Cl-γCF_3 with chlorine and trifluoromethyl end groups give a power conversion efficiency (PCE) of over 17% which is the highest among polymer solar cells processed by halogen-free solvents. Dissymmetric chlorination and trifluoromethylation is a practical approach towards a low band-gap acceptor for eco-compatible processed photovoltaic applications.